International Journal of Mass Spectrometry 295 (2010) 36–42

Contents lists available at ScienceDirect

International Journal of Mass Spectrometry

journal homepage: www.elsevier.com/locate/ijms

Photodissociation and DFT investigation of $V^+(C_2H_4)_n$ (n = 1–3) complexes

Jinyun Yuan, Zeng-Guang Zhang, Yuchao Zhao, Gao-Lei Hou, Hong-Guang Xu, Weijun Zheng*

Beijing National Laboratory for Molecular Science, State Key Laboratory of Molecular Reaction Dynamics, Institute of Chemistry, Chinese Academy of Sciences, Zhongguancun North First Street 2, Beijing 100190, PR China

ARTICLE INFO

Article history:
Received 5 February 2010
Received in revised form 21 June 2010
Accepted 21 June 2010
Available online 1 July 2010

Keywords:
Mass spectrometry
Mass-selection
Photodissociation
Vanadium–ethene complex

ABSTRACT

$V^+(C_2H_4)_n$ were produced in a supersonic molecular beam by laser vaporization and were mass-analyzed with a reflectron time-of-flight mass spectrometer. $V^+(C_2H_4)_n$ (n = 1–3) are predominant mass peaks in the mass spectrum. These species were mass-selected and photodissociated with 1064, 532 and 355 nm photons. Dissociation occurs by elimination of neutral ethene molecules. The fragment ion yields were studied as a function of photon fluxes in order to give insight into the dissociation mechanisms. The geometric structures, bond dissociation energies and ground electronic state of $V^+(C_2H_4)_n$ (n = 1–4) were investigated using density functional theory (DFT). It has been confirmed that the most stable structures of $V^+(C_2H_4)_n$ are all in quintet states.

1. Introduction

Reactions of transition-metal cations with small hydrocarbon molecules in the gas phase have attracted extensive interest from the past decades. The studies of metal ion–hydrocarbon complexes have important applications in heterogeneous and homogeneous catalysis, microelectronics, organometallic chemistry, and biochemistry [1]. Consequently, great effort has been made to investigate reaction mechanisms of metal ions with hydrocarbon and the structures of metal–hydrocarbon complexes. A large number of experimental investigations had been reported [2–13]. Metz group reported photodissociation spectroscopy of $Au^+(C_2H_4)$ and $Pt^+(C_2H_4)$ using a dual time-of-flight photofragment spectrometer, and the upper limits to metal–ligand bond strengths of 28,800 cm^{-1} (3.57 eV) and 19,200 cm^{-1} (2.38 eV) were obtained [7]. Armentrout and coworkers measured the first and second adiabatic metal ion ethene bond energies of $M^+(C_2H_4)_n$ (M = Ti–Cu, n = 1–2) by guided ion beam mass spectrometry [8]. The structures and bond dissociation energies of $Al^+(C_2H_4)$ were determined by Schwarz and coworkers using Fourier-transform ion cyclotron resonance mass spectrometry and ab initio calculations [9]. Kleiber and coworkers conducted photodissociation spectroscopy of $Mg^+(C_2H_4)$, $Ca^+(C_2H_4)$, $Al^+(C_2H_4)$ and $Zn^+(C_2H_4)$ on a reflectron time-of-flight mass spectrometer [10–13].

Theoretical results were also reported to explain the experiments. Bauschlicher and coworkers studied the bonding of the first-row transition-metal positive ions and Nb^{2+} cation to ethene molecule early in 1990s [14,15]. They found that V^+ bounds to ethene molecule electrostatically. Castleman group proposed the mechanisms of the reactions between $(V_2O_5)_n^+$ (n = 1–2) and ethene based on density functional theory calculations [16]. Sicilia and coworkers studied the adsorption properties of ethene, vinyl, acetic acid, and acetate species on the PdAu alloys surface by the density functional cluster model approach in 2009 [17]. In the same year, by means of density functional theory, Honkala group investigated the reaction pathways for different processes involving the hydrogenation–dehydrogenation, decomposition and isomerization of organic moieties derived from ethene on Pd(1 1 1) and (2 1 1) surfaces [18]. Although many studies of reactions of metal cations with ethene have been performed [7–14,19–25], to our knowledge, there is no report on laser-induced dissociation of $V^+(C_2H_4)_n$ complexes.

Ethene is an important intermediate in many industrially relevant processes such as in acetylene hydrogenation and the synthesis of vinyl acetate [26]. The interaction of ethene with metal can lead to different reactions like ethene hydrogenation, decomposition, and polymerization [18]. The selectivity for each of these reactions depends on the nature of the metals and the experimental conditions [26–31]. Photodissociation experiments studies of gas-phase complex ions can provide information on stability, possible structures, interaction bonding and dissociation mechanisms [32]. In this work, we combine laser photodissociation experiments with DFT calcula-

* Corresponding author. Tel.: +86 10 62635054; fax: +86 10 62563167.
E-mail address: zhengwj@iccas.ac.cn (W. Zheng).

1387-3806/$ – see front matter © 2010 Elsevier B.V. All rights reserved.
doi:10.1016/j.ijms.2010.06.018

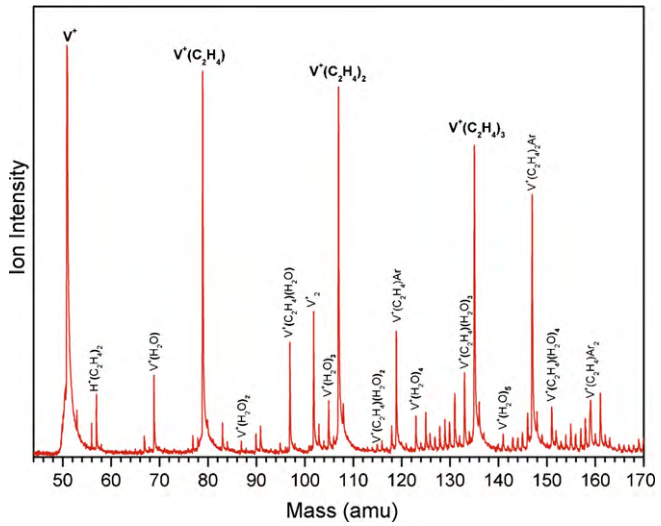

Fig. 1. Mass spectrum distribution of vanadium–ethene cationic complexes.

tions to investigate the metal–ligand bonding and structures of $V^+(C_2H_4)_n$.

2. Experimental and computational methods

2.1. Experimental

The experiments were conducted on a home-built reflectron time-of-flight mass spectrometer (RTOF-MS), which has been described elsewhere [33]. Briefly, the V^+ cations were produced in the source chamber by ablating a rotating, translating vanadium disc target (13 mm diameter) using the second harmonic output (532 nm, 10 mJ/pulse, 5 pulse/s) of a Nd:YAG laser, while argon gas with 3–5 atm backing pressure seeded with ethene molecules (~4%) was allowed to expand through a pulsed valve over the vanadium target (General Valve Series 9). The produced vanadium–ethene complexes were then extracted in the direction perpendicular to the cluster beam, and accelerated to about 1.2 keV. Two sets of deflectors and einzel electrostatic lenses were used to focus the ion beam on the first space focus point, and then the ions were reflected by a reflector and detected by a dual microchannel plate (MCP) detector installed at the second space focus region. The output signals were amplified and digitized with a 100 MHz digital oscilloscope card, and were collected in a laboratory computer with the home-made software. The timing of the laser vaporization, electric pulse acceleration and recording were adjusted with a digital delay pulse generator (DG645, Stanford Research System, Inc.).

For the photodissociation experiments, a deceleration–dissociation–reacceleration method was used. The cluster ions to be photodissociated were mass-selected with a mass gate installed at the first space focus region of RTOF-MS and were decelerated with deceleration plates located right after the mass gate, then they were photodissociated with another Nd:YAG laser (Continuum Surelite II-10) at 1064, 532, and 355 nm, respectively. The fragment ions and surviving parent ions were all reaccelerated toward the reflectron plates, and then reflected to the dual MCP (microchannel plate) detector. It should be noticed that the photodissociation region selected is near the first space focus region, different from the photodissociation region at the turning point of RTOF-MS which has been used extensively by some experimental groups [34–37]. Our experimental results show that it is more convenient to cross the laser beam with the ion beam near the first space focus region, and the mass peaks of the fragment ions and parent ion were well separated with this deceleration–dissociation–reacceleration method.

2.2. Computational methods

All calculations were performed with the density functional theory (DFT) using the hybrid B3LYP [38–41] exchange-correlation functional as implemented in the software package Gaussian03 [42]. 6-311 + G (d, p) basis set was employed for all calculations. As we know that DFT has been widely utilized and is an efficient tool for studying molecular properties, especially compounds of transition metal [43]. It has also been shown that DFT calculations can provide a relatively precise description of the metal–ligand interactions [44]. In this work, configurations of $V^+(C_2H_4)_n$ (n = 1–4) and their corresponding neutral complexes were fully optimized. Vibration frequencies were calculated for all the optimized geometric structures in order to verify that they were real local minima on the potential surfaces. The calculations confirmed that those optimized geometry structures all have no imaginary frequency. The zero-point vibrational energy corrections and basis set superposition error are included for the total energies. The

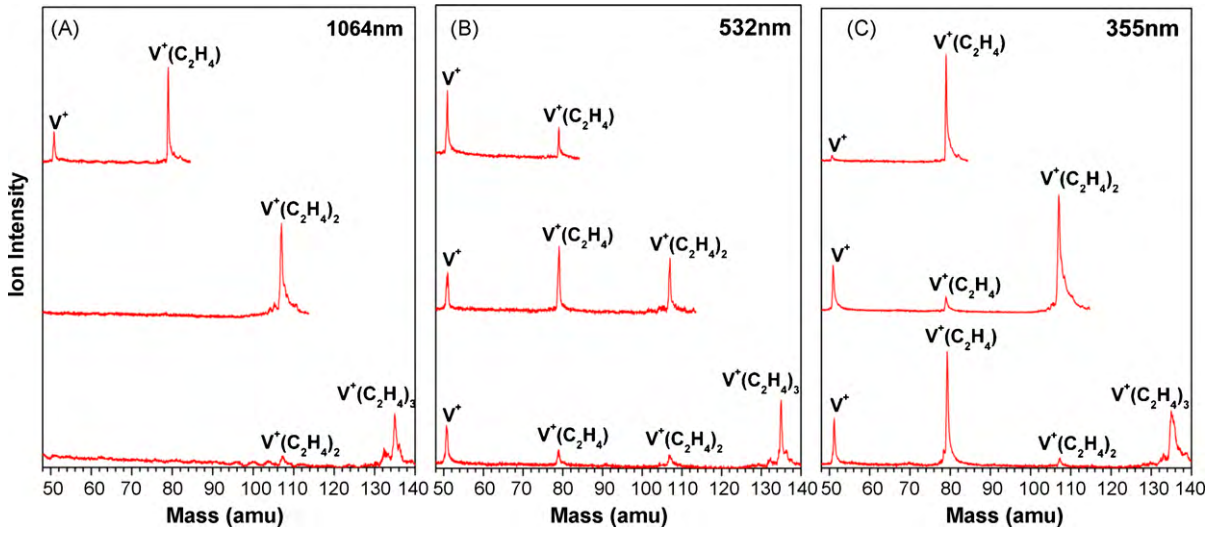

Fig. 2. Photodissociation mass spectra of $V^+(C_2H_4)_n$ (n = 1–3) at 1064, 532, and 355 nm with laser fluences of 152, 84 and 27 mJ/pulse, respectively.

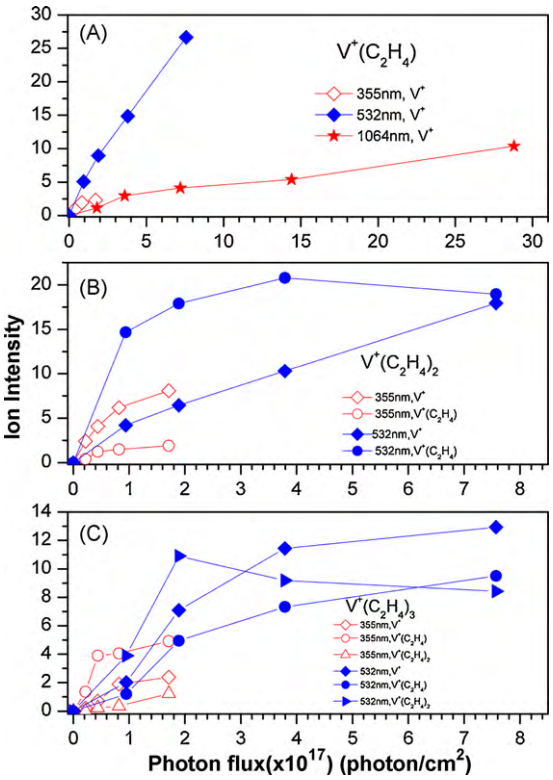

Fig. 3. Intensities of fragment ions from $V^+(C_2H_4)_n$ (n = 1–3) as a function of photon fluxes (1064, 532 and 355 nm, respectively).

bond dissociation energies of $V^+(C_2H_4)_n$ (n = 1–4) were also calculated.

3. Results and discussion

3.1. Experimental

Fig. 1 shows a typical mass spectrum of vanadium–ethene complexes obtained in our experiments. The predominant mass peaks on the spectrum are $V^+(C_2H_4)_n$ (n = 1–3). The mass peaks of $V^+(C_2H_4)_nAr$ (n = 1–2) can be also observed. In addition, the appearance of the mass peaks of $V^+(H_2O)_m$ and $V^+(C_2H_4)_n(H_2O)_m$ are due to the existence of the trace amounts of water molecules in the carrier gas. Interestingly, although the mass peaks of $V^+(C_2H_4)_{1-3}$ are quite intense, very little signal is observed at m/z = 163, indicating that $V^+(C_2H_4)_4$, if it was produced at all, was produced much less efficiently than $V^+(C_2H_4)_{1-3}$.

In order to understand the interaction of vanadium cation with ethene and the relative stabilities of the $V^+(C_2H_4)_n$ (n = 1–3), the photodissociation experiments were performed using 1064, 532 and 355 nm photons. The photofragment mass spectra of $V^+(C_2H_4)_n$ (n = 1–3) are shown in Fig. 2. The unique dissociation channel is loss of intact ethene molecules. The intensities of fragment ions were studied as a function of photon fluxes at the wavelengths of 1064, 532 and 355 nm. Fig. 3 illustrates the relationship between the intensities of fragment ions and photon fluxes at the three wavelengths.

3.1.1. Photodissociation of $V^+(C_2H_4)$

From Fig. 2, we can know that the unique photodissociation channel of $V^+(C_2H_4)$ is losing one neutral ethene molecule leaving V^+ for three wavelengths, 1064, 532 and 355 nm. Fig. 3(A) indicates that the relationship between photon fluxes and the intensity of fragment ion yields is nearly linear for the three wavelengths. Therefore, it is likely that single photon absorption occurs for $V^+(C_2H_4)$ photodissociation at 1064, 532 and 355 nm wavelengths. From Fig. 3(A), it can be seen that the photodissociation efficiency is the highest at 532 nm and the lowest at 1064 nm.

3.1.2. Photodissociation of $V^+(C_2H_4)_2$

No fragment was observed for $V^+(C_2H_4)_2$ photodissociation at the wavelength 1064 nm (Fig. 2(A)). For the dissociation of $V^+(C_2H_4)_2$ with 532 nm photons, Fig. 2(B) indicates that the intensity of fragment ion $V^+(C_2H_4)$ is higher than that of fragment ion V^+, and also Fig. 3(B) shows that the efficiency of generating $V^+(C_2H_4)$ is higher than that of generating V^+ at all different photon fluxes of 532 nm. The above facts mean that generating $V^+(C_2H_4)$ is the main dissociation path of $V^+(C_2H_4)_2$, and the fragment V^+ might be generated by losing one ethene molecules from the fragment $V^+(C_2H_4)$ or losing two ethene molecules from parent $V^+(C_2H_4)_2$ with low photodissociation efficiencies. Fig. 3(B) also depicts that the curve of fragment $V^+(C_2H_4)$ first goes up and then goes down, indicating the survival of fragment ion $V^+(C_2H_4)$ decreases. This feature of the curve of fragment $V^+(C_2H_4)$ is perhaps due to secondary dissociation of fragment $V^+(C_2H_4)$ at 532 nm. Fig. 2(C) shows the photodissociation spectra of $V^+(C_2H_4)_n$ (n = 1–3) at 355 nm. For the parent $V^+(C_2H_4)_2$, the fragment ion V^+ peak is much higher than the fragment $V^+(C_2H_4)$, and Fig. 3(C) shows that the efficiency of generating V^+ is higher than that of generating $V^+(C_2H_4)$ at all different photon fluxes of 355 nm. So we can confirm that the dissociations of $V^+(C_2H_4)_2$ at 355 nm is mainly losing two ethene molecules from parent $V^+(C_2H_4)_2$.

3.1.3. Photodissociation of $V^+(C_2H_4)_3$

For the photodissociation of $V^+(C_2H_4)_3$, only a very weak $V^+(C_2H_4)_2$ fragment ion peak is observed at 1064 nm (Fig. 2(A)). For 532 and 355 nm wavelengths, Fig. 2(B) and (C) shows that the three fragments, $V^+(C_2H_4)_2$, $V^+(C_2H_4)$ and V^+ from parent $V^+(C_2H_4)_3$ were observed. Figs. 2(B) and 3(C) show that V^+ is the main photofragment of $V^+(C_2H_4)_3$ dissociated at high 532 nm photon flux. With 355 nm photons (Fig. 2(C)), it is obvious that the parent $V^+(C_2H_4)_3$ has the tendency losing two ethene molecules to produce fragment $V^+(C_2H_4)$.

3.2. Theoretical results and discussion

3.2.1. Structures of $V^+(C_2H_4)_n$(n = 1–4)

Vanadium–ethene complexes $V^+(C_2H_4)_n$ (n = 1–4) of singlet, triplet and quintet states were calculated using DFT method. The neutral species of $V(C_2H_4)_n$ (n = 1–4) of doublet, quartet and sextet states were also calculated. The atomic spectra data of NIST Database [45] show that the ^3F and ^1G states of V^+ are 1.10 and 2.22 eV above the ground state (^5D). Our calculation found that the triplet (^3F) and singlet (^1G) states of V^+ are 1.04 and 2.53 eV higher than the quintet (^5D) in energy, in agreement with the experimental data. The atomic spectra data [45] also show that the sextet (^6D) and doublet (^2G) states of V atom are 0.28 and 1.36 eV higher than the ground state (^4F). Our calculations found the doublet state of V atom is 1.73 eV above the ground state (^4F), which is also consistent with the experimental data. Our calculations found the sextet state is 0.18 eV lower than the quartet state, which is off from the experimental data by 0.46 eV. Over all, the theoretical calculations are consistent with the atomic spectra data except the relative energy of V atom sextet state to the ground state has been underestimated by 0.46 eV. The calculated ionization energy of vanadium atom and ethene molecule are 6.53 and 10.50 eV, respectively, in agreement with the experimental values (6.75 and 10.51 eV) in the literature [46,47], indicating that the theoretical method used here is appropriate for vanadium–ethene systems. Many initial structures for both neutral and cationic $V^+(C_2H_4)_n$ (n = 1–4) were considered, and

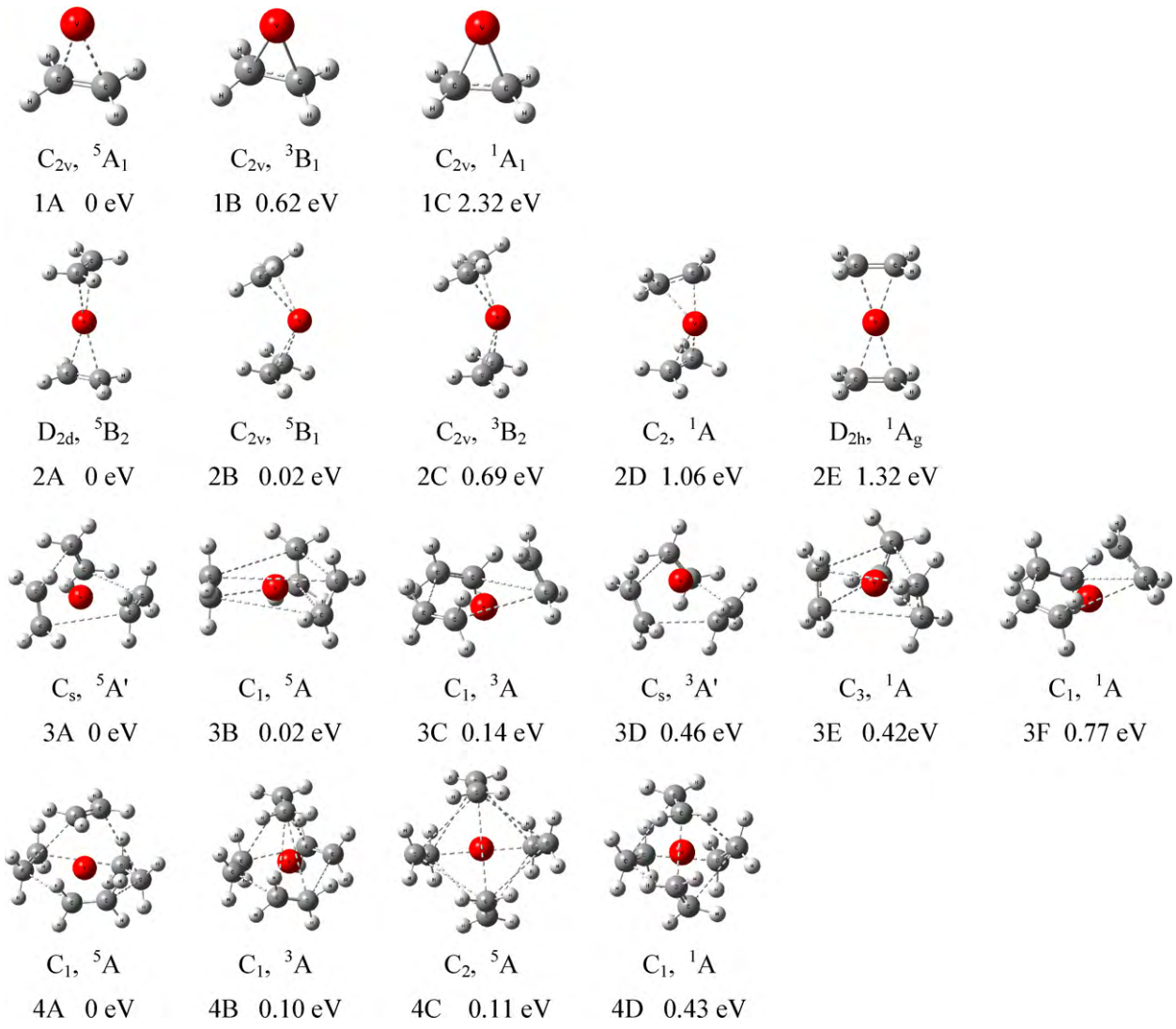

Fig. 4. Structures of stable isomers and their relative energies of $V^+(C_2H_4)_n$ (n = 1–4) in quintet, triplet and singlet states.

the optimized structures for $V^+(C_2H_4)_n$ ions (n = 1–4) at the stationary points with the multiplicities of singlet, triplet and quintet states are depicted in Fig. 4. From the relative energy, it is clear that all the most stable structures of $V^+(C_2H_4)_n$ (n = 1–4) have multiplicity of 5. Our calculations also found that the neutral $V(C_2H_4)_n$ (n = 1–4) in quartet state are generally more stable than those in doublet and sextet states except that the sextet state of $V(C_2H_4)_2$ is 0.09 eV lower than the quartet state.

Our calculations demonstrate that the most stable structure of $V^+(C_2H_4)$ is a $^5A_1$ Π-complex with C_{2v} symmetry (Fig. 4) in agreement with the calculations of Bauschlicher and coworkers [15]. In addition, we also found that $V^+(C_2H_4)$ has a $^5A_2$ state, almost identical in energy and structure to the $^5A_1$ state. In both states, the vanadium cation approaches to the Π-bond along the line perpendicular to the C=C bond. The C=C bond (1.36 Å) in $V^+(C_2H_4)$ is elongated by 0.03 Å relative to the free ethene molecule (1.33 Å) calculated at the same level. The V–C distance (2.37 Å) is much longer than V–C bond distance (1.85 Å) in VC_2^+ cluster calculated at the same level by Redondo et al. [48]. Consequently, we infer that V^+ and ethene forms complexes by electrostatic interaction as suggested by Bauschlicher and coworkers [15], and $V^+(C_2H_4)$ has a *T-shaped* structure as defined by Stringer et al. [7], in which the V atom interacts with the C=C bond but does not form bonds with the carbon atoms. The dihedral angle of HCCH changes from 180° to 167.6°, which implies that the hydrogen atoms bend away from the ethene molecule plane to reduce the repulsion from the vanadium cation. Different from the structures of quintet state, the singlet and triplet states of $V^+(C_2H_4)$ have *metallocyclopropane* type structure [7], in which V–C bonds are formed. The C-C distances in singlet and triplet states of $V^+(C_2H_4)$ are 1.43 and 1.41 Å, longer than the C=C bond. The structure of neutral $V(C_2H_4)$ also has C_{2v} symmetry, however, its C=C bond (1.46 Å) is much longer than that of the free ethene molecule (1.33 Å) and the V–C bond (2.06 Å) is shorter than that (2.37 Å) of cationic $V^+(C_2H_4)$. It indicates that the Π-bond of ethene is considerably weakened in the neutral $V(C_2H_4)$ structure [7]. The configuration of neutral $V(C_2H_4)$ is a *metallocyclopropane* type structure in which the V atom form V–C bonds with the two carbon atoms to make a three-membered ring. The hydrogen atoms deviate much from the ethene molecule plane, so carbon atom is nearly sp^3 hybridization in neutral $V(C_2H_4)$.

There are two isomers (2A and 2B) for $V^+(C_2H_4)_2$ cation in quintet state. Isomer 2A has D_{2d} symmetry with the two ethene molecules positioned on opposite sides of V^+ and aligned perpendicular to one another (Fig. 4). The two C=C bond lengths of isomer 2A are both 1.35 Å and its four V–C bonds are all 2.40 Å. Isomer 2B has C_{2v} symmetry and is only 0.02 eV higher than isomer 2A in energy. The two C=C bond lengths of isomer 2B are both 1.36 Å and its four V–C bond are all 2.38 Å. Similarly, the neutral $V(C_2H_4)_2$

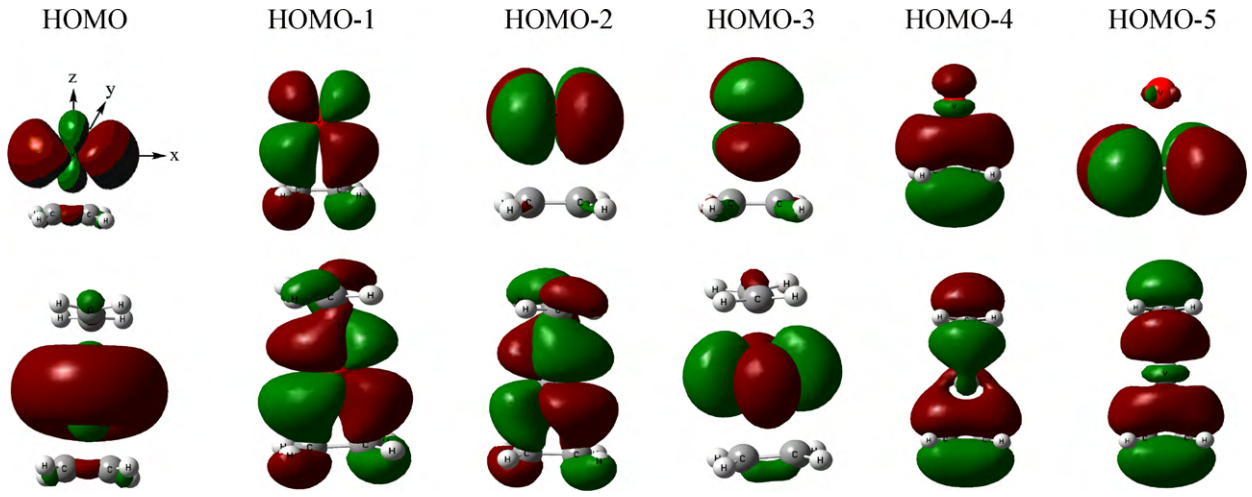

Fig. 5. Frontier molecular orbitals of the most stable isomers of $V^+(C_2H_4)_n$ (n = 1–2) (the structures in the left column in Fig. 4).

has two isomers corresponding to those of the cation. One has two ethene molecules positioned on opposite sides of V atom and the two C=C bonds are perpendicular. The point group of the structure is C_{2v} with $^4B_1$ ground electronic state, different from its cationic structure with D_{2d} point group. In this neutral structure, the two C=C bond lengths are different in which one is 1.46 Å, the other is 1.37 Å. The distances between the two ethene molecules and V atom are also different. The V–C distances for the first ethene molecule are 2.08 Å, and those for the second ethene molecule are 2.33 Å. The second isomer of neutral $V(C_2H_4)_2$ has C_{2v} symmetry with $^4B_2$ state. Its energy is 0.25 eV higher than the first isomer. In this neutral isomer, the V-ethene distances for the two ethene molecules are the same and the two C=C bonds are both 1.42 Å. The V–C distances for the two carbon atoms in the same ethene molecule are not even, one is 2.18 Å while the other is 2.22 Å. From structural analysis above, we confirm that the C=C bonds of ethene molecule in $V(C_2H_4)_2$ neutral are longer than those in $V^+(C_2H_4)_2$ cation. The V–C bonds in $V(C_2H_4)_2$ neutral are shorter than those in the cationic $V^+(C_2H_4)_2$.

$V^+(C_2H_4)_3$ has two isomers (3A and 3B) in quintet state in which the three ethene molecules are all Π-bonded to the vanadium cation. The most stable isomer 3A has C_s symmetry with two equivalent ethene molecules and one different ethene molecule. Isomer 3B has C_1 symmetry and is only 0.02 eV higher than isomer 3A in energy. For the neutral $V(C_2H_4)_3$, it also has two isomers. Similarly, the C=C bonds in $V^+(C_2H_4)_3$ are shorter than those in $V(C_2H_4)_3$ neutral, and the V–C bonds in $V^+(C_2H_4)_3$ are longer than those in neutral $V(C_2H_4)_3$.

$V^+(C_2H_4)_4$ also has two isomers (4A and 4C) in quintet state with all four ethene molecules Π-bonded to the V^+. Isomer 4A has C_1 symmetry with ^5A electronic ground state. In this isomer, three ethene molecules surround V^+ and the last one is on the top of V^+. Isomer 4C has C_2 symmetry with 0.11 eV higher in energy than that of isomer 4A. We also calculated the structures of $V(C_2H_4)_4$ neutral in quartet state, and the results show that the C=C bonds in the neutral are slightly longer than those in $V^+(C_2H_4)_4$, and the V–C bonds in the neutral are shorter than those in $V^+(C_2H_4)_4$ cation, which is in agreement with the results of $V(C_2H_4)_{1-3}$.

3.2.2. The Frontier molecular orbital analysis of vanadium cation with ethene molecules

The bonding in $V^+(C_2H_4)_n$ can be described by the Dewar–Chatt–Duncanson model [49,50]. The model presents that the ligand donates electrons from its HOMO (the Π orbital of C_2H_4) to the σ-type metal orbital, and then the metal back-donates electrons from d orbital into anti-bonding ligand orbital (the Π* orbital of C_2H_4). Fig. 5 depicts the frontier molecular orbitals of the most stable isomers of $V^+(C_2H_4)_n$ (n = 1–2), in which HOMO, HOMO-1, HOMO-2 and HOMO-3 are singly occupied while HOMO-4 and HOMO-5 are fully occupied. To aid the discussion conveniently, we define that the origin of the coordinate is at the position of V atom, the x axis is parallel to one of the C=C bond, and the z axis aligns with V atom and the center of C=C bond. For $V^+(C_2H_4)$, HOMO is associated with the hybridization of $3d_{x^2-y^2}$, 4s and $3d_{z^2}$ orbitals of vanadium atom. HOMO-1 is from the interaction between Π* anti-bonding orbital of ethene molecule and $3d_{xz}$ orbital of vanadium cation. The electron shifts from the 3d orbital of vanadium to the Π* orbital of ethene molecule, thus, weakens the C=C bond slightly. HOMO-2 is mainly contributed by the $3d_{xy}$ orbital of vanadium cation. HOMO-3 is mainly contributed by $3d_{yz}$ orbital of vanadium cation. HOMO-4 is mainly composed by the Π-orbital of ethene molecule with small amount of contribution from the 4 s, $3p_z$ and $3d_{z^2}$ orbitals of vanadium cation. For $V^+(C_2H_4)_2$, HOMO is due to the hybridization of 4s and $3d_z{}^2$ orbitals of vanadium atom. HOMO-1 is from the interaction between Π* anti-orbital of ethene molecule and the $3d_{yz}$ orbital of vanadium cation. HOMO-2 is from the interaction between Π* anti-orbital of ethene molecule and $3d_{xz}$ orbital of vanadium cation. HOMO-3 is mainly contributed by $3d_{x^2-y^2}$ orbital of vanadium cation. HOMO-4 is mainly composed by the Π-orbital of ethene molecule with small amount of contribution from the $3p_z$ and $3d_{x^2-y^2}$ orbitals of vanadium cation. For both $V^+(C_2H_4)$ and $V^+(C_2H_4)_2$, HOMO-5 is mainly localized on the ethene molecules. The Π-bond of ethene is only slightly perturbed by the V cation.

3.2.3. Bond dissociation energies

In order to investigate the relative stability and photodissociation mechanisms of $V^+(C_2H_4)_n$ (n = 1–3), we calculated the Bond Dissociation Energies (BDEs) of $V^+(C_2H_4)_n$ based on the energies of the most stable structures in quintet state. The results are summarized in Table 1. The BDEs are defined by Eq. (1).

$$\mathrm{BDE} = -(E_{V^+(C_2H_4)_n} - E_{V^+(C_2H_4)_{n-1}} - E_{C_2H_4}) \quad (1)$$

3.2.3.1. $V^+(C_2H_4)$. The BDE of $V^+(C_2H_4)$ was calculated to be 1.09 eV by Bauschlicher and coworkers [15]. The theoretical BDE of $V^+(C_2H_4)$ in this work is 1.34 eV, which is 0.25 eV higher than Bauschlicher's value and 0.05 eV higher than the experimental value (1.29 ± 0.08 eV) measured by Armentrout and coworkers with guided ion beam mass spectrometry [8], indicating reasonable

Table 1
Bond dissociation energies (BDEs) and electronic states for the most stable structures of $V^+(C_2H_4)_n$ (n = 1–4).

	State	Theoretical BDE (eV)	Experimental BDE[a] (eV)
$V^+(C_2H_4)$	$^5A_1$	1.34 (−0.06)[b]	1.29 ± 0.08
$V^+(C_2H_4)_2$	$^5B_2$	1.12 (−0.08)	1.32 ± 0.14
$V^+(C_2H_4)_3$	$^5A'$	0.76 (−0.08)	
$V^+(C_2H_4)_4$	^5A	0.51 (−0.08)	

[a] Ref. [8].
[b] The theoretical BDEs shown here are after ZPE and BSSE corrections. The numbers in parentheses show the differences between corrected and uncorrected values.

agreement between them. Based on the value measured by Armentrout et al., a single photon (1.16 eV) of 1064 nm should not be able to induce the dissociation of $V^+(C_2H_4)$, which is inconsistent with our experimental results (Figs. 2(A) and 3(A)). The possible explanation for the above contradiction is that the experimental value measured by Armentrout et al. is only 0.13 eV higher than the photon energy of 1064 nm, the dissociation of $V^+(C_2H_4)$ with 1064 nm could be happened by the help of the internal energies of $V^+(C_2H_4)$ left due to $V^+(C_2H_4)$ being not cooled enough in the experiments. We estimated the average internal energy of $V^+(C_2H_4)$ at 298 K to be ~0.19 eV, which is large enough to contribute to the dissociation of $V^+(C_2H_4)$ at 1064 nm. On the other hand, absorption of two 1064 nm photons might also cause dissociation of $V^+(C_2H_4)$. That possibility cannot be completely ruled out. The energies of 532 nm and 355 nm photons are 2.33 and 3.50 eV, respectively, much higher than the BDE of $V^+(C_2H_4)$, therefore, the single photon of 532 nm or 355 nm is able to peel off an intact ethene molecule from $V^+(C_2H_4)$ complex, as shown in Fig. 3(A).

3.2.3.2. $V^+(C_2H_4)_2$. The calculated BDE for $V^+(C_2H_4)_2$ is 1.12 eV, lower than the photon energy 1.16 eV of 1064 nm. But our experimental results (Fig. 2(A)) show that $V^+(C_2H_4)_2$ cannot be dissociated by 1064 nm photon. Armentrout and coworkers [8] found that the BDE of $V^+(C_2H_4)_2$ is higher than that of $V^+(C_2H_4)$. Our experimental results are somewhat in agreement with their experimental results. It seems the bond dissociation energy of $V^+(C_2H_4)_2$ from our theoretical calculations is inconsistent with Armentrout's guided ion beam experiments and our own dissociation experiments at 1064 nm. The non-dissociation of $V^+(C_2H_4)_2$ by 1064 nm photon might be explained by the following. Firstly, multiple-photon dissociation of $V^+(C_2H_4)_2$ at 1064 nm did not happen. Secondly, it might be possible that $V^+(C_2H_4)_2$ cannot absorb 1064 nm photons. Thirdly, it is possible that the BDE of $V^+(C_2H_4)_2$ is actually higher than the photon energy 1064 nm photons as suggested by reference [8]. Based on our experiments (Fig. 2(B)), a 532 nm photon (2.33 eV) is able to eliminate one or two ethene molecules from $V^+(C_2H_4)_2$. The theoretical results show that the photon energy of 355 nm is enough for eliminating two ethene molecules from $V^+(C_2H_4)_2$. It is in agreement with the experiments (Fig. 2(C)).

3.2.3.3. $V^+(C_2H_4)_3$. The calculated BDE of $V^+(C_2H_4)_3$ is about 0.76 eV. The single photon energy of 1064 nm is only enough to eliminate one ethene molecule from $V^+(C_2H_4)_3$, which is compatible with the experiments. The single photon energy of 532 nm (2.33 eV) is enough to eliminate one or two ethene molecules from $V^+(C_2H_4)_3$. Fig. 3(C) shows when the photon flux is lower than 2×10^{17} photons/cm^2, $V^+(C_2H_4)_2$ is the main product. As the photon flux increases, $V^+(C_2H_4)$ becomes the main product and the amount of fragment V^+ also increases. This feature of the curve indicates that some of the $V^+(C_2H_4)$ fragments are secondary product from fragment $V^+(C_2H_4)_2$. The single 532 nm photon is not able to eliminate three ethene molecules from $V^+(C_2H_4)_3$. Thus, the fragment V^+ might be resulted from two photon absorption of $V^+(C_2H_4)_3$ in two steps: (1) $V^+(C_2H_4)_3$ absorbs the first photon to produce $V^+(C_2H_4)$ (major) or $V^+(C_2H_4)_2$ (minor); (2) $V^+(C_2H_4)$ or $V^+(C_2H_4)_2$ absorbs the second photon to generated V^+ cation. With the energy of 355 nm photon (3.50 eV), the fragments $V^+(C_2H_4)_2$, $V^+(C_2H_4)$ and V^+ are all possible to be generated from parent $V^+(C_2H_4)_3$ by single photon absorption, in good agreement with the experiment results (Fig. 2(C)).

3.2.3.4. $V^+(C_2H_4)_4$. Our calculations show that the BDE of $V^+(C_2H_4)_4$ is about 0.51 eV, which means $V^+(C_2H_4)_4$ is stable. However, our calculations also demonstrate that the ΔG at 298 K for the reaction $V^+(C_2H_4)_3 + C_2H_4 \rightarrow V^+(C_2H_4)_4$ is only −0.01 eV. More likely, the temperature in our source is over 298 K due to the imperfect cooling by molecule beam expansion. That can probably explain the low production or non-observation of $V^+(C_2H_4)_4$ in our experiments.

4. Conclusions

The complexes obtained from the reactions of vanadium cation with ethene molecules were studied in the gas phase using mass spectrometry, laser photodissociation experiments and DFT calculations. $V^+(C_2H_4)_n$ (n = 1–3) are the predominant ion peaks in the mass spectrum. The photodissociation of parent $V^+(C_2H_4)$ at 1064, 532 and 355 nm wavelengths produced only V^+ fragment. For the photodissociation of $V^+(C_2H_4)_2$, two fragments V^+ and $V^+(C_2H_4)$ were generated at 532 and 355 nm; yet, no fragment is observed at 1064 nm. The single 1064 nm photon is able to remove one ethene molecule from parent ion $V^+(C_2H_4)_3$. The main dissociation channel of parent $V^+(C_2H_4)_3$ at 532 nm is eliminating two ethene molecules by the first photon followed by desorption of the last ethene molecule by the second photon. For the dissociation of $V^+(C_2H_4)_3$ at 355 nm, eliminating two ethene molecules is the main channel. Our calculations show that $V^+(C_2H_4)_n$ (n = 1–4) are more stable in quintet state than in singlet and triplet states. Analysis of frontier molecular orbital and BDEs shows that vanadium cation can interact with ethene molecules through electrostatic interaction, and the Π-bonds of the ethene molecules are only slightly perturbed.

Acknowledgments

This work was supported by the Natural Science Foundation of China (NSFC, Grant No. 20933008). We are grateful to Professor Zhen Gao for discussions. We thank the anonymous reviewers for their valuable comments.

Appendix A. Supplementary data

Supplementary data associated with this article can be found, in the online version, at doi:10.1016/j.ijms.2010.06.018.

References

[1] W.Y. Lu, R.G. Liu, T.H. Wong, J. Chen, P.D. Kleiber, J. Phys. Chem. A 106 (2002) 725.
[2] P.B. Armentrout, Acc. Chem. Res. 28 (1995) 430.
[3] J.C. Weisshaar, Acc. Chem. Res. 26 (1993) 213.
[4] J.C. Weisshaar, Adv. Chem. Phys. 82 (1992) 213.
[5] B.S. Freiser, Acc. Chem. Res. 27 (1994) 353.
[6] B.S. Freiser, J. Mass. Spectrom. 31 (1996) 703.
[7] K.L. Stringer, M. Citir, R.B. Metz, J. Phys. Chem. A 108 (2004) 6996.
[8] M.R. Sievers, L.M. Jarvis, P.B. Armentrout, J. Am. Chem. Soc. 120 (1998) 1891.
[9] D. Stockigt, J. Schwarz, H. Schwarz, J. Phys. Chem. 100 (1996) 8786.
[10] J. Chen, T.H. Wong, Y.C. Cheng, K. Montgomery, P.D. Kleiber, J. Chem. Phys. 108 (1998) 2285.
[11] J.H. Holmes, P.D. Kleiber, D.A. Olsgaard, K.H. Yang, J. Chem. Phys. 112 (2000) 6583.
[12] J. Chen, T.H. Wong, P.D. Kleiber, K.H. Yang, J. Chem. Phys. 110 (1999) 11798.

[13] W.Y. Lu, P.D. Kleiber, M.A. Young, K.H. Yang, J. Chem. Phys. 115 (2001) 5823.
[14] C.W. Bauschlicher, S.R. Langhoff, H. Partridge, J. Phys. Chem. 95 (1991) 6191.
[15] M. Sodupe, C.W. Bauschlicher, S.R. Langhoff, H. Partridge, J. Phys. Chem. 96 (1992) 2118.
[16] N.A. Moore, R. Mitric, D.R. Justes, V. Bonacic-Koutecky, A.W. Castleman, J. Phys. Chem. B 110 (2006) 3015.
[17] I. Rivalta, G. Mazzone, N. Russo, E. Sicilia, J. Chem. Theory Comput. 5 (2009) 1350.
[18] J. Andersin, N. Lopez, K. Honkala, J. Phys. Chem. C 113 (2009) 8278.
[19] M.K. Geoffrey, B.K. Mark, J. Chem. Phys. 107 (1997) 10555.
[20] F. Huisken, B. Kohn, R. Alexandrescu, I. Morjan, J. Chem. Phys. 113 (2000) 6579.
[21] T. Zhixin, T. Zichao, Rapid Commun. Mass Spectrom. 19 (2005) 2893.
[22] C. Berg, T. Schindler, M. Kantlehner, G. Niedner-Schatteburg, V.E. Bondybey, Chem. Phys. 262 (2000) 143.
[23] J. Hrusak, R.H. Hertwig, D. Schroeder, P. Schwerdtfeger, W. Koch, H. Schwarz, Organometallics 14 (1995) 1284.
[24] L. Sanders, S.D. Hanton, J.C. Weisshaar, J. Chem. Phys. 92 (1990) 3498.
[25] R.H. Hertwig, W. Koch, D. Schroder, H. Schwarz, J. Hrusak, P. Schwerdtfeger, J. Phys. Chem. 100 (1996) 12253.
[26] C.F. Bartholomew, R. Farrauto, Fundamentals of Industrial Catalysis, Wiley, New York, 2006.
[27] D.B. Teschner, J. Borsodi, A. Wootsch, Z. Revay, M. Havecker, A. Knop-Gericke, S.D. Jackson, R. Schlogl, Science 320 (2008) 86.
[28] A. Molnar, A. Sarkany, M. Varga, J. Mol. Catal. A 173 (2001) 185.
[29] Z. Ma, F. Zaera, Surf. Sci. Rep. 61 (2006) 229.
[30] Y. Segura, N. Lopez, J. Perez-Ramirez, J. Catal. 247 (2007) 383.
[31] F. Studt, F. Abild-Pedersen, T. Bligaard, R.Z. Sorensen, C.H. Christensen, J.K. Norskov, Science 320 (2008) 1320.
[32] S.E. Kooi, A.W. Castleman, J. Phys. Chem. A 103 (1999) 5671.
[33] Y.C. Zhao, Z.G. Zhang, J.Y. Yuan, H.G. Xu, W.J. Zheng, Chin. J. Chem. Phys. 22 (2009) 655.
[34] Y.-S. Yang, C.-S. Yeh, Chem. Phys. Lett. 305 (1999) 395.
[35] J. Husband, F. Aguirre, P. Ferguson, R.B. Metz, J. Chem. Phys. 111 (1999) 1433.
[36] D.S. Cornett, M. Peschke, K. Laihing, P.Y. Cheng, K.F. Willey, M.A. Duncan, Rev. Sci. Instrum. 63 (1992) 2177.
[37] L.N. Ding, M.A. Young, P.D. Kleiber, W.C. Stwalley, A.M. Lyyra, J. Phys. Chem. 97 (1993) 2181.
[38] A.D. Becke, Phys. Rev. A 38 (1988) 3098.
[39] A.D. Becke, J. Chem. Phys. 98 (1993) 5648.
[40] C. Lee, W. Yang, R.G. Parr, Phys. Rev. B 37 (1988) 785.
[41] P.J. Stephens, F.J. Devlin, C.F. Chabalowski, M.J. Frisch, J. Phys. Chem. A 98 (1994) 11623.
[42] M.J.T. Frisch, G.W. Trucks, H.B. Schlegel, G.E. Scuseria, M.A. Robb, J.R. Cheeseman, V.G. Zakrzewski, J.A. Montgomery Jr., R.E. Stratmann, J.C. Burant, S. Dapprich, J.M. Millam, A.D. Daniels, K.N. Kudin, M.C. Strain, O. Farkas, J. Tomasi, V. Barone, M. Cossi, R. Cammi, B. Mennucci, C. Pomelli, C. Adamo, S. Clifford, J. Ochterski, G.A. Petersson, P.Y. Ayala, Q. Cui, K. Morokuma, D.K. Malick, A.D. Rabuck, K. Raghavachari, J.B. Foresman, J. Cioslowski, J.V. Ortiz, A.G. Baboul, B.B. Stefanov, G. Liu, A. Liashenko, P. Piskorz, I. Komaromi, R. Gomperts, R.L. Martin, D.J. Fox, T. Keith, M.A. Al-Laham, C.Y. Peng, A. Nanayakkara, M. Challacombe, P.M.W.J.B. Gill, W.W.M.W. Chen, J.L.G.C. Andres, M. Head-Gordon, E.S. Replogle, J.A. Pople, Gaussian 03, Gaussian Inc., Pittsburgh, PA, 2003.
[43] H.Y. Huang, J. Padin, R.T. Yang, Ind. Eng. Chem. Res. 38 (1999) 2720.
[44] T. Ziegler, Chem. Rev. 91 (1991) 651.
[45] Y. Ralchenko, A.E. Kramida, J. Reader, NIST ASD Team, NIST Atomic Spectra Database (version 3.1.5) [Online]. Available: http://physics.nist.gov/asd3. National Institute of Standards and Technology, Gaithersburg, MD, 2008.
[46] A.M. James, P. Kowalczyk, E. Langlois, M.D. Campbell, A. Ogawa, B. Simard, J. Chem. Phys. 101 (1994) 4485.
[47] K. Ohno, K. Okamura, H. Yamakado, S. Hoshino, T. Takami, M. Yamauchi, J. Phys. Chem. 99 (1995) 14247.
[48] P. Redondo, C. Barrientos, A. Largo, Int. J. Mass Spectrom. 263 (2007) 101.
[49] M.J.S. Dewar, G.P. Ford, J. Am. Chem. Soc. 101 (1979) 783.
[50] D.M.P. Mingos, J. Organomet. Chem. 635 (2001) 1.